RSC Advances

PAPER

View Article Online
View Journal | View Issue

Cite this: *RSC Adv.*, 2014, **4**, 45266

Molecularly imprinted TiO_2 hybridized magnetic Fe_3O_4 nanoparticles for selective photocatalytic degradation and removal of estrone

Shoufang Xu,[ab] Hongzhi Lu,[a] Lingxin Chen*[b] and Xiaochuan Wang*[c]

Received 4th July 2014
Accepted 15th September 2014

DOI: 10.1039/c4ra06632d

www.rsc.org/advances

As a widely used photocatalyst, titania (TiO_2) enjoys significant advantages; however, it faces the severe challenge of poor selectivity. And interestingly, molecular imprinting gains great popularity, owing to its desired recognition specificity. Herein, by using estrone as a template molecule, we prepared molecularly imprinted TiO_2 hybridized magnetic ferroferric oxide (Fe_3O_4) nanoparticles through a semi-covalent approach by a liquid phase deposition method, for selective photocatalytic degradation and removal of target estrone with the irradiation of UV light. The obtained Fe_3O_4@SiO_2@imprinted TiO_2 displayed high adsorption capacity, fast kinetics and high selectivity. In the presence of 10 times of coexisting nontarget compounds, the apparent rate constant, k_{app}, for photodegradation of target estrone over the hybridized nanoparticles, was about 6 times of that over net TiO_2. Also, excellent stability during long-time photocatalysis was exhibited. More importantly, the Fe_3O_4@imprinted TiO_2 provided potential application prospectives for photocatalytic removal of trace target organic pollutants in the presence of high-level pollutants.

1. Introduction

With the fast development of industrialization, more and more pollutants are poured into the natural environment, which results in increasingly serious environmental pollution, especially water pollution. Among the organic pollutants, estrone, bisphenol A, tetrabromobisphenol A and 4-nonylphenol *etc.*, with similar structural features and estrogenic activity, are classified as phenolic environmental estrogens (PEEs).[1] Because PEEs are fat-soluble and can easily be enriched in the human body, they have become the focus of attention in recent years. As one of the naturally occurring PEEs, estrone has carcinogenic properties and adverse environmental effects.[2] Various methods, such as physicochemical treatment,[3] biological degradation,[4] and photocatalytic degradation[5] have been developed to remove organic pollutants in the aquatic environment. Among those methods, photocatalytic degradation using titania (TiO_2) has been well studied for environmental protection. Nevertheless, TiO_2 photocatalysts possess two severe defects: first, it is as yet difficult to realize selective removal of harmful low-level pollutants in the presence of high-level less harmful pollutants because of the poor selectivity; second, TiO_2 nanoparticle is difficult to reuse because of small particle size. Several approaches have been proposed to enhance the selectivity of TiO_2. One approach is to control the surface's electric charge by adjusting pH:[6] a lower pH is helpful for the degradation of negatively charged contaminants, and a higher pH is favorable for the degradation of positively charged contaminants. The other way is to modify the surface of TiO_2 with specific molecules which can obtain a selective and effective adsorption.[7] In recent years, molecularly imprinted polymers (MIPs), owing to their attractive selectivity, have been introduced to improve the selectivity of the TiO_2 photocatalyst.[8–10]

Commonly, MIPs are prepared by copolymerization of functional monomers and cross-linkers in the presence of target analytes which act as template molecules. After removal of template, recognition sites complementary in size, shape, and functionality to the template are formed in the three-dimensional polymer network.[11,12] MIPs as versatile materials have aroused extensive attention for diverse species in various fields.[11–15] Coating MIPs on the surface of TiO_2 to improve the selectivity of catalytic degradation is an important aspect.[8–10] Nowadays, three main methods have been proposed to prepared MIPs coated TiO_2 photocatalyst. The first one involves coating organic MIPs layer on TiO_2 particles, in which TiO_2 acts as photocatalyst, and the layer of MIPs shows specific affinity toward target compounds.[9] However, this approach involves a multistep procedure, and organic MIPs would be destroyed after longtime photocatalysis. To avoid such drawbacks, some

[a]*School of Chemistry and Chemical Engineering, Linyi University, Linyi 276005, China. E-mail: xshfang1981@163.com*

[b]*Key Laboratory of Coastal Zone Environmental Processes and Ecological Remediation, Yantai Institute of Coastal Zone Research, Chinese Academy of Sciences, Yantai 264003, China. E-mail: lxchen@yic.ac.cn; Fax: +86 535 2109130; Tel: +86 535 2109130*

[c]*Key Laboratory of Ecological Geochemistry, Ministry of Land and Resources, National Research Center for Geoanalysis, Beijing 100037, China. E-mail: wangwxc@iccas.ac.cn; Tel: +86 10 68999579*

studies are focused on coating inorganic MIPs on the surface of TiO_2 by sol–gel process. For example, Shen *et al.* prepared Al^{3+}-doped diethyl phthalate molecularly imprinted TiO_2@SiO_2 nanocomposite particles.[10] However, TiO_2 were embedded into highly cross-linked MIPs which resulted in relatively low photocatalytic degradation ability. It can be hypothesized that the selective photocatalytic degradation ability of TiO_2 would be greatly increased if TiO_2 film acts as both photocatalyst and imprinted recognition layer. So, directly imprinting TiO_2 might be an efficient way, which can be achieved by liquid phase deposition (LPD) method.[16]

LPD is known as a soft-solution process for direct preparation of metal oxide thin film on various substrates from aqueous solutions, by means of a ligand-exchange equilibrium reaction between the metal–fluoro complex ions and metal oxide.[16] The addition of boric acid as a scavenger for F^- ions can shift the chemical equilibrium, resulting in the deposition of metal oxide homogeneously onto substrates.[16] Using $(NH_4)_2TiF_6$ as the precursor, TiO_2 films would be deposited. LPD method has been used for protein imprinting[17–19] and selective photocatalysis by molecular imprinted TiO_2 thin films[16] because of its significant advantages especially the mild reaction condition.

In the present work, we proposed to prepare new molecularly imprinted TiO_2 photocatalyst for highly selective photodegradation and removal of estrone by LPD on the surface of magnetic ferroferric oxide (Fe_3O_4) nanoparticles. Fe_3O_4 was introduced for its magnetic separation ability, SiO_2 film was coated on the surface of Fe_3O_4 nanoparticles beneficial for immobilizing target estrone, and LPD was employed for the formation of footprint cavities on the TiO_2 film. With the irradiation of UV light, the obtained Fe_3O_4@SiO_2@imprinted TiO_2 could selectively adsorb and photodegrade estrone in aqueous media. The properties of prepared photocatalyst, including molecular binding capacity, recognition specificity and degradation mechanism/kinetics, were investigated in detail. By combining the separation ability of Fe_3O_4 particles with the functional capability of MIPs and TiO_2, the photocatalyst supply perspective applications to simple, rapid, high-efficiency degradation and removal of trace targeted pollutants in the presence of high level non-target pollutants.

2. Experimental

2.1. Materials and apparatus

$FeCl_3 \cdot 6H_2O$, ethylene glycol, NaAc and polyethylene glycol for preparation of magnetic Fe_3O_4 were obtained from Shanghai Chemical Reagent Company. Dibutyltin dilaurate (DBDU), 3-isocyanatopropyltriethoxysilane (IPTS) and tetraethoxysilicane (TEOS) for modification of Fe_3O_4 were supplied also by Shanghai Chemical Reagent Company. P25 TiO_2 nanoparticles (anatase, hydrophilia) (P25), ammonium hydroxide (25%), hexafluorotitanate $(NH_4)_2TiF_6$, boric acid, estrone, bisphenol A (BPA) and phenol were provided by Tianjin Chemical Reagent Co., Ltd. Tetrahydrofuran (THF, 99%, Tianjin Jiangtian Chemicals, China) was refluxed over sodium and then distilled. All the chemicals were of analytical reagent grade and used as received without further purification except specified.

Morphological observation of nanoparticles was performed by transmission electron microscopy (TEM; JEOL, JEM-1230, Japan). The surface diffractogram of the deposited TiO_2 was characterized by X-ray diffraction on an X'Pert PRO X-ray diffractometer with a Cu Ka radiation source (XRD, PANalytical, Netherlands). A FT-IR spectrometer (Thermo Nicolet Corporation, USA) was employed to examine the infrared spectra of samples using a pressed KBr tablet. Brunauer–Emmett–Teller (BET) surface area was determined by nitrogen adsorption/desorption at 77 K using a Micromeritics ASAP 2020 Sorptometer (Micromeritics, ASAP 2020, USA). The samples were degassed in a vacuum at 180 °C prior to adsorption measurements. UV-visible spectra were obtained by a Thermo Scientific NanoDrop 2000/2000c spectrophotometer (Thermo, USA) supplied with a quartz cell. The concentrations of each pollutant in the mixture were analyzed by HPLC equipped with a C_{18} ODS column (250 mm × 4.6 mm, 5 μm) and DAD detector (Elite Instrument Inc., China).

2.2. Preparation and modification of Fe_3O_4

Fe_3O_4 microspheres were synthesized by solvothermal method as reported.[20] Fe_3O_4 modified with IPTS were prepared according to the previous method with a little modification.[21] Briefly, 0.10 g of Fe_3O_4 particles were treated with 50 mL 0.1 M HCl aqueous solution by ultrasonication for 10 min, then separated and washed with deioned water. After homogeneously redispersed in the mixture of 80 mL of ethanol, 20 mL of deioned water and 1.0 mL of ammonia aqueous solution (28 wt%), 2 mL of TEOS was added followed by stirring at room temperature for 6 h. And then1 mL of IPTS was added, and the solution was further reacted for 18 h at room temperature. Then Fe_3O_4@SiO_2 microspheres modified with IPTS were separated and washed with ethanol and water.

2.3. Preparation of estrone imprinted TiO_2 layer on Fe_3O_4

Before deposition TiO_2 layer on the surface of Fe_3O_4@SiO_2, template estrone was first immobilized on the surface of Fe_3O_4@SiO_2 by the reaction of isocyanate group of IPTS and phenol moiety of estrone, forming a thermally cleavable urethane bond as reported.[22] The urethane bond is stable at room temperature, but reversible cleavage occurs at elevated temperatures. Briefly, 0.2 g Fe_3O_4@SiO_2 modified with IPTS was dispersed in 50 mL of dried THF. To the solution, 5 mmol estrone was added at room temperature, followed by the addition of 0.3 mL DBDU, and then the reaction mixture was refluxed for 24 h under nitrogen atmosphere. After reaction, magnetic particles were separated and washed with ethanol.

LPD solution was prepared by dissolving ammonium hexafluorotitanate (0.15 mmol) and boric acid (0.3 mmol) into 1 mL deionized water. Then ammonia aqueous solution was added to adjust the pH to 7.0. The LPD solution (1 mL), P25 TiO_2 nanoparticles (0.04 g L^{-1}) were added to 5.0 mL of 1.0 mg mL^{-1} Fe_3O_4 particles immobilized with estrone water solution, and then the mixture was mildly shaken for 3 h at 25 °C. The resultant magnetic particles were washed several times with deionized water. Subsequently, the imprinted estrone was

removed by calcination at 400 °C, which produced the molecularly imprinted TiO_2 hybridized Fe_3O_4 nanoparticles (Fe_3O_4@SiO_2@imprinted TiO_2), that is, MIPs for simplicity. As control materials, the non-imprinted polymers (NIPs) were also prepared as described above but without the addition of template estrone.

2.4. Binding property studies of the MIPs

Molecular binding properties of the MIPs including static adsorption, kinetic adsorption and selective binding capacity were estimated by a batch procedure method. The procedures were carried out as follows. MIPs particles with the mass of 30 mg were dispersed in 5 mL of estrone solutions of various concentrations. After shaking at room temperature for 24 h, the samples were separated, and the concentrations of which were determined using HPLC-DAD. HPLC conditions employed for estrone were as follows: mobile phase, methanol–water (80 : 20, v/v); flow rate, 1.0 mL min^{-1}; room temperature; DAD detection, at 280 nm; injection volume, 20 μL. The calibration curves for the detection of estrone was obtained by performing a linear regression analysis ranging from 2.0 to 75 mg L^{-1}. Good linearity was obtained with correlation coefficients of $R > 0.99$. The limits of detection (LOD) were 1.5 ng based on a signal-to-noise ratio of 3. Precision calculated in terms of intraday repeatability ($n = 6$) and interday reproducibility (6 different days) was 2.4% and 3.5% respectively.

The binding amount of estrone was determined by subtracting the residual amount of estrone in solution from the total estrone amount. Meanwhile, the binding kinetics was tested by monitoring the temporal amount of estrone in the solutions. Selectivity experiments were carried out by using BPA and phenol as structural analogs.

2.5. Photocatalytic degradation experiments

The photocatalytic degradation experiments were performed in a 250 mL of ringent photoreactor with stirring at room temperature, in which 40 mL of 10 mg L^{-1} estrone water solution and 100 mg of photocatalysts were added. A circular 20 W UV light with an emission peak at 254 nm was horizontally positioned 10 cm above the surface of the solution. After immersion for 6 h to achieve the adsorption–desorption equilibrium, the concentrations of the pollutant were determined as the initial concentration, and then the photo-irradiation was started. At different time intervals, 2 mL aliquots were sampled to detect the pollutants.

3. Results and discussion

3.1. Preparation and characterization of the estrone imprinted Fe_3O_4@SiO_2@TiO_2 (MIPs)

The widely adopted technique for preparing MIPs is non-covalent approach, in which aprotic and low polar organic solvents are often used. However, the non-covalent imprinted polymers often show poor recognition ability for the target in aqueous environment because the hydrogen bond formed between template and functional monomer can be disturbed by the polar solvent. In this work, LPD method involved in aqueous solution was employed for estrone imprinting, and the obtained MIPs were used to remove organic pollutants in aqueous environment. In order to achieve ideal molecular imprinting in aqueous environment, semi-covalent approach[23] was adopted.

The synthesis procedure for estrone MIPs by semi-covalent approach is illustrated in Scheme 1A, which involves synthesis of Fe_3O_4 magnetic nanoparticles, silica-shell coating, template immobilization, TiO_2 imprinted film deposition and template removal. Hydrophilic Fe_3O_4 nanoparticles with uniform morphology and high magnetization were prepared by solvothermal method. Then SiO_2 shell with isocyanate group was coated on the surface of Fe_3O_4 by sol–gel process beneficial for immobilization of template. Template estrone was immobilized on the surface of Fe_3O_4 by covalent urethane bond formed between isocyanate group of IPTS and phenol moiety of estrone. Then TiO_2 film was deposited on the surface of Fe_3O_4 and calcination was used for removing template to form imprinted recognition sites. For the pure semi-covalent imprinting method, template estrone was only immobilized on the surface of Fe_3O_4@SiO_2, and the thickness of the TiO_2 shell is about 40 nm (Fig. 1), which resulted in low binding capacity and mass transfer rate. So in the improved scheme, template also was added in the liquid phase deposition solution, and recognition sites can be formed in the whole TiO_2 layer, as illustrated in Scheme 1A. The binding capacity and mass transfer can be enhanced in this improved scheme. The reason of choosing TiO_2 as the molecularly imprinted layer was that TiO_2 can achieve photocatalytic degradation of pollutant. Furthermore, the LPD method is suitable for imprinting because of its mild reaction conditions. Calcination was used to remove the template because reversible cleavage of the urethane bond formed between an isocyanate and a phenol occurs at elevated temperatures.[23]

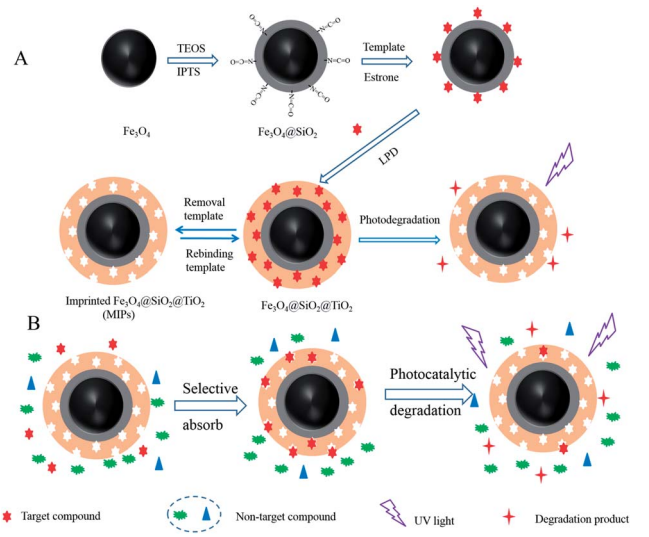

Scheme 1 The Schematic illustrations for preparation estrone imprinted TiO_2 films on the surface of magnetic Fe_3O_4 nanoparticles (A) and the possible mechanism of selective photocatalyst degradation of target template by imprinted Fe_3O_4@SiO_2@TiO_2 (B).

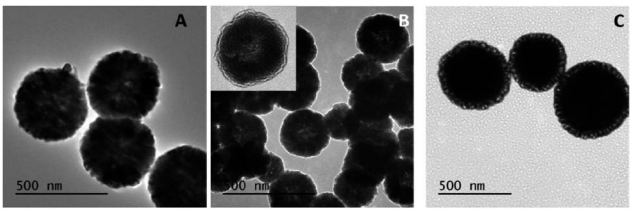

Fig. 1 TEM images of Fe_3O_4 (A), Fe_3O_4@SiO_2 (B) and imprinted Fe_3O_4@SiO_2@TiO_2 (C).

TEM images of Fe_3O_4, Fe_3O_4@SiO_2 and imprinted Fe_3O_4@SiO_2@TiO_2 were shown in Fig. 1. All samples displayed spherical shape. Fig. 1A shows the uncoated Fe_3O_4 microsphere displayed relatively uniform size distribution with the diameter about 400 nm. Fig. 1B shows the Fe_3O_4 microspheres were fully coated by silica shell with thickness about 10 nm. Fig. 1C clearly shows the uniform core-shell structure of Fe_3O_4@SiO_2@TiO_2, and the thickness of the TiO_2 shell was about 40 nm. So, it can be confirmed from TEM pictures that TiO_2 layer was successfully deposited on the surface of Fe_3O_4.

The preparation procedure was also estimated by FT-IR, as shown in Fig. 2. Compared with Fe_3O_4 (a), the Fe_3O_4@SiO_2 (b) and Fe_3O_4@SiO_2–estrone (c) clearly displayed the characteristic peaks of stretch vibration of Si–O–Si (the strong peaks at 1090 cm^{-1}), indicating the formation of silica film. The peaks at 1718 cm^{-1} ascribed to C=O and 1636 cm^{-1} ascribed to amine groups (c) indicated the formation of urethane bonds between Fe_3O_4@SiO_2 and estrone, suggesting that the template estrone was immobilized on the surface of Fe_3O_4@SiO_2 particles. After deposited TiO_2 film (d), the strong peaks at 1090 cm^{-1} disappeared. Meanwhile, the C=O peaks at 1718 cm^{-1} disappeared, confirming the removal of template estrone and the presence of the molecularly imprinted sites.

The magnetic hysteresis loops and the dispersion and agglomeration process of Fe_3O_4 nanoparticles and the imprinted Fe_3O_4@SiO_2@TiO_2 were illustrated in Fig. 3. The shape of magnetic hysteresis loop of MIPs was similar to the Fe_3O_4 nanoparticles while the saturation magnetization value was slightly lower than that of the latter. The MIPs homogeneously dispersed in water could go straight towards the magnet and adhere to the inner side wall of the vials when external magnetic field was applied, and the turbid solution became clear and transparent. The results showed that the obtained materials could be separated and collected effectively and simply.

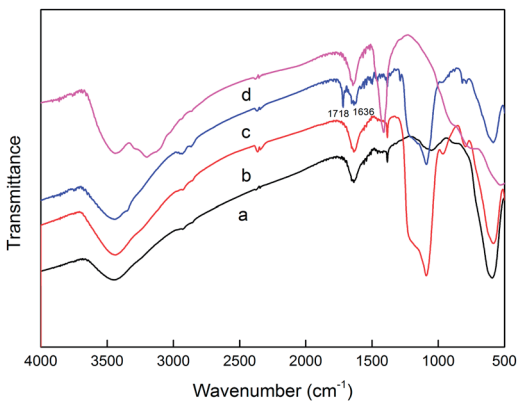

Fig. 2 The FT-IR spectra of (a) Fe_3O_4; (b) Fe_3O_4@SiO_2; (c) Fe_3O_4@SiO_2–estrone and (d) Fe_3O_4@SiO_2@imprinted TiO_2.

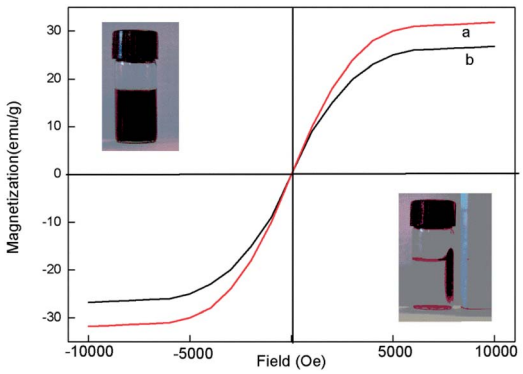

Fig. 3 Magnetic hysteresis loops of Fe_3O_4 nanoparticles (a) and Fe_3O_4@SiO_2@TiO_2 (b), and the insets show the dispersion (upper) and agglomeration (below) process of the Fe_3O_4@SiO_2@TiO_2 nanoparticles.

3.2. Binding properties of the MIPs

Binding capacity is an important index to evaluate the performances of MIPs. Binding properties including static adsorption equilibrium, binding kinetics and binding selectivity were evaluated by batch adsorption experiments. Static adsorption experiments were first performed in order to evaluate the adsorption capacities of MIPs at concentrations of 0–100 mg L^{-1} from aqueous solutions and the results were displayed in Fig. 4A. As seen, the amounts of estrone adsorbed per unit mass of MIPs increased with the increase of initial concentrations of estrone. At higher equilibrium concentration than 60 mg L^{-1}, the adsorption capacity became stable. Also as observed, the adsorption capacity of MIPs was about 4 times of NIPs and P25. There were no specific recognition sites in NIPs and P25, so their binding capacities were relatively low. Moreover, it was found the binding capacity of P25 was slightly higher than that of NIPs, which might well because that the particle size of P25 (diameter 25 nm, surface area 53.5 m^2 g^{-1}) was smaller than NIPs (diameter 380 nm, surface area 46.7 m^2 g^{-1}).

The Scatchard equation was employed to evaluate the maximum binding capacity of the MIPs, expressed as eqn (1):

$$\frac{Q}{C_e} = \frac{Q_{max}}{K_d} - \frac{Q}{K_d} \quad (1)$$

where Q stands for the binding capacity (mg g^{-1}), K_d represents the equilibrium dissociation constant (mg L^{-1}), Q_{max} (mg g^{-1}) is the theoretical maximum adsorption amount of template molecules on polymers, and C_e (mg mL^{-1}) is the equilibrium concentration of template in the solution. According to the slope and intercept of the Scatchard plot, namely the

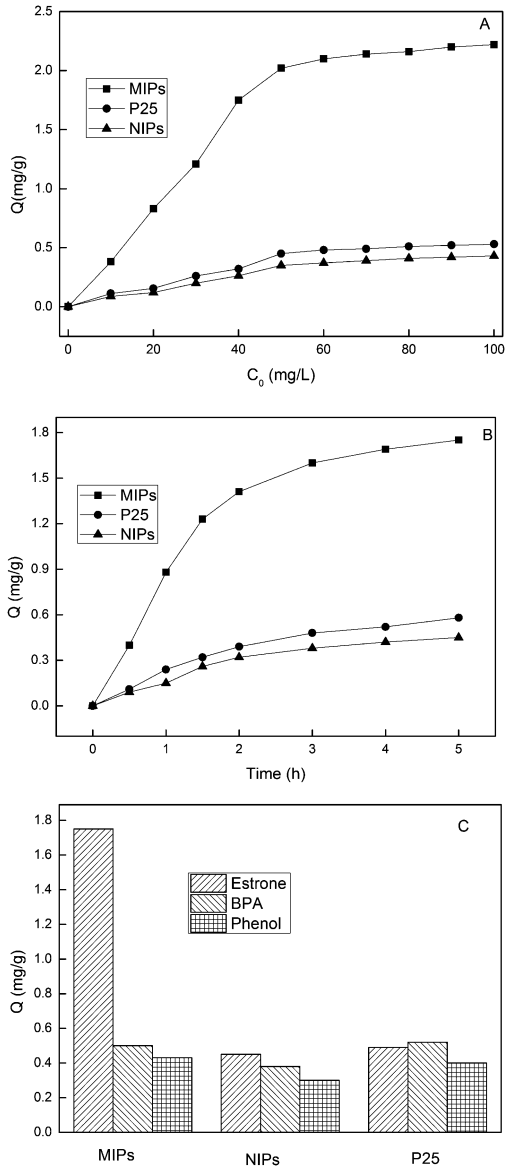

Fig. 4 Binding isotherms of MIP for estrone in water, which including the static adsorb experiment (A), kinetic uptake experiment (B) and selective binding experiment (C). Experimental conditions for static adsorb experiment: $V = 5.0$ mL; mass of adsorb materials (MIP, P25 and NIP), 30 mg; adsorption time, 24 h. Experimental conditions for kinetic uptake experiment: $V = 5.0$ mL; $C_0 = 40$ mg L^{-1}; mass of adsorb materials (MIP, P25 and NIP), 30 mg. Experimental conditions for selective binding experiment: mass of adsorb materials (MIP, P25 and NIP), 30 mg; $C_0 = 40$ mg L^{-1}; $V = 5.0$ mL; adsorption time, 24 h; room temperature.

relationship between Q/C_e and Q, K_d and Q_{max} for the MIPs were calculated to be 0.1003 mg L^{-1} and 2.62 mg g^{-1}, respectively.

Fig. 4B shows the time dependent evolutions of estrone amount bound by MIPs, NIPs and P25. It was observed that the adsorption amounts of estrone onto the three materials increased with time. MIPs took up 50% of the equilibrium adsorption amount during 1 h and nearly reached saturation state within 4 h. And, more importantly, to attain the same adsorption capacity (the equilibrium adsorption capacity of NIPs or P25), MIP required only one eighth of time required by NIPs or P25. Hence, the MIPs had fast binding kinetics.

In order to investigate the competitive recognition ability of MIPs, two structural analogues of BPA and phenol were employed. As seen from Fig. 4C, the NIPs and P25 presented similar binding capacities for the three compounds. However, the binding capacity of MIPs for estrone was much higher than that for two analogues. The results showed that there were no selective recognition sites in NIPs and P25, while selective recognition sites existed in MIPs. MIPs could selectively bind estrone from other phenols, which opened a promising way to selective extraction and photodegradation of estrone.

3.3. Photodegradation of estrone

It is well known that the anatase TiO_2 has higher photocatalytic degradation ability than rutile TiO_2. So before carrying out the photodegradation experiments, the crystal forms of the deposited TiO_2 were characterized by XRD, and the results were displayed in Fig. 5. As seen from Fig. 5a, the P25 TiO_2 nanoparticles (anatase, hydrophilia) were the mixture of anatase and rutile. The dominant peaks at 2θ of 25.3°, 37.9°, 48.0°, 53.9°, 55.1° and 62.7° were corresponding to the (101), (004), (200), (105), (211), and (204) reflection of anatase TiO_2, respectively, while the peaks at 2θ of 27.4°, 36.1° and 69.0° corresponding to the (110), (101) and (301) reflections of rutile phase. From Fig. 5b–e, we can see without calcination, the deposited TiO_2 did not show anatase crystal form (cure b and d), so the step of calcination was necessary. Compared with TiO_2 deposited in the absence of P25 (cure c), the TiO_2 deposited in the presence of P25 (cure e) was more similar to anatase TiO_2. Thus, in order to realize photodegradation, P25 was used as crystallization revulsant and calcination was carried out to complete conversion of the crystalline.

The photodegradation experiments were carried out in single systems (one organic substrate in the suspension) and

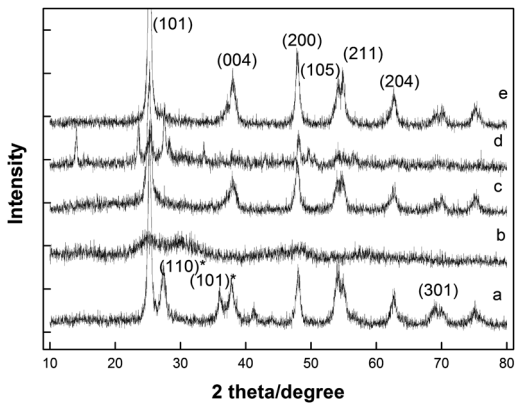

Fig. 5 XRD patterns of the imprinted TiO_2 films. (a) P25 TiO_2 nanoparticles (anatase, hydrophilia) purchased from Tianjin Chemical Reagent Co., Ltd. (b) TiO_2 deposited in the absence of P25 and without calcine; (c) TiO_2 deposited in the absence of P25 and calcined at 300 °C for 3 h; (d) TiO_2 deposited in the presence of P25 without calcine and (e) TiO_2 deposited in the presence of P25 and calcined at 300 °C for 3 h.

binary systems (coexisting two pollutants in the suspension). Fig. 6A shows the kinetic data for photodegradation of estrone over different photocatalysts in single systems. The kinetic data showed that all the degradation processes followed the first-order kinetics as eqn (2):

$$-\ln\left(\frac{C_t}{C_0}\right) = k_{\text{app}}t \quad (2)$$

where k_{app} is the apparent reaction rate constant, which can be used to measure the degradation rate. The results indicated that the direct photolysis without photocatalyst was not so efficient for estrone. The k_{app} value of the target estrone over MIPs was 0.069 min^{-1}, being 363% of that over NIPs (0.019 min^{-1}) and 238% of that over P25 (0.029 min^{-1}), respectively.

Fig. 6B shows the kinetic data for the photodegradation of different phenols by MIPs in the single systems. The k_{app} value of BPA and phenol over MIPs were 0.021 and 0.017 min^{-1}, being only 30.4% and 24.6% of that estrone over, respectively. The degradation of the target estrone was remarkably enhanced by the MIPs layer while the degradation of the non-target pollutant was correspondingly depressed by the MIPs coating. This enhanced photocatalytic selectivity can be attributed to molecule selective adsorption on the MIPs coatings. Notably, the ratio of k_{target} to $k_{\text{non-target}}$ increased with the concentration decrease of the organic compounds. This indicated that the selectivity of MIPs was further improved when the initial concentration of the target pollutant was decreased, which would be especially in favor of selectively removing the low-level target pollutant in the presence of high-level non-target pollutants.

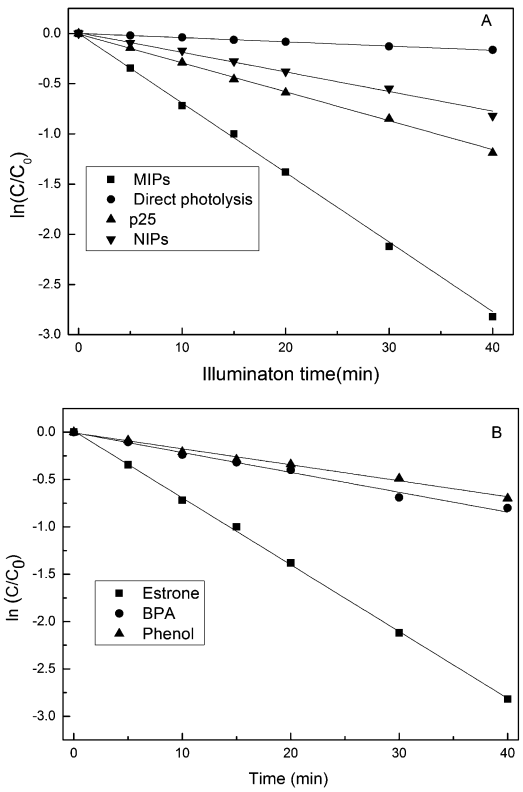

Fig. 6 Kinetic data for photocatalytic degradation of estrone with different photocatalyst (A); and photocatalytic degradation of different phenols with imprinted Fe_3O_4@SiO_2@TiO_2 (B) The initial concentration of each organic compound was 10 mg L^{-1}.

Binary system photocatalysis degradation experiments were also carried out to assess the selective photocatalysis degradation ability of MIPs. As seen from Table 1, the k_{app} values for the target's degradation over the MIPs were greater than those over P25, and the k_{app} values for the coexisted non-target over the MIPs were smaller than those over P25. And more importantly, R, the ratios of k_{app} values ($k_{\text{target}}/k_{\text{nontarget}}$) over MIPs were much higher than those over P25. The results of binary system further confirmed that MIPs enhanced the photocatalytic selectivity towards the target contaminant. That MIPs enhanced the degradation of target estrone and depressed that of nontarget pollutants is very likely because a large number of selective recognition sites existed in the surface of MIPs. The high sensitivity would facilitate differentiating targeted estrone from coexistent compounds during their photocatalytic degradation and thereby realize highly selective photocatalytic degradation and removal of estrone.

The MIPs displayed high selectivity in the photocatalytic removal of low-level target pollutants in the presence of high-level other pollutants. This can be explained as schematically shown in Scheme 1B. The whole photodegradation procedure includes two steps: first, the target compounds should be sufficiently adsorbed by TiO_2, and then those adsorbed compounds were photodegradated. The adsorption of targeted compounds onto the photocatalyst might be the rate determining step, which could be deduced from Fig. 4B and 6 (the kinetics of estrone adsorption on MIPs (about 5 h) was lower than the photocatalytic degradation of estrone over Fe_3O_4@SiO_2@TiO_2 (about 1 h)). When the slowest step in the degradation process was enhanced, the total degradation process would be greatly accelerated. For the MIPs, many specific recognition sites existing in TiO_2 layer facilitated the adsorption of target template molecules. So, the absorption rate of target molecules was higher than that of those non-target compounds, as well as the absorption rate of MIPs was higher than that of NIPs. The tendency was in good agreement with the photodegradation ability. The advantage of "preferential adsorption and preferential degradation" was more obvious when the concentration of target was low or the structure difference between target molecules and non-target molecules was large. Therefore, the enhanced photocatalyic selectivity can be attributed to molecularly selective adsorption on the MIPs coatings. The view agreed well with some reported works.[7,16,24] Considering the difference between natural water and standard solutions studied above, photodegradation of estrone in real water samples, like tap water, underground water and river water were also studied. The water samples were collected in Nalgene bottles and filtered through 0.45 μm pore size membrane to remove the suspended particles before use. Initially, estrone was not detected in real water sample, so standard addition method was adopted to spike estrone into the real water samples. The results of photodegradation of estrone in real water samples in the presence and absence of non-target

Table 1 Rate constants (k_{app}/min^{-1}) for the photocatalytic degradation of target pollutant (estrone 5.0 mg L^{-1}) in the presence of coexisted compounds over imprinted Fe_3O_4@SiO_2@TiO_2 and P25[a]

	Imprinted Fe_3O_4@SiO_2@TiO_2 (MIPs)			P25		
Coexisted compounds	k_{target} ($\times 10^3$)	$k_{non\text{-}target}$ ($\times 10^3$)	R	k_{target} ($\times 10^3$)	$k_{non\text{-}target}$ ($\times 10^3$)	R
Estrone	85 ± 2	—		0.026 ±	—	
1× BPA	67 ± 3	19 ± 4	3.5	15 ± 1	23 ± 2	0.65
1× Phenol	73 ± 3	21 ± 3	3.5	17 ± 2	27 ± 2	0.63
10× BPA	61 ± 2	11 ± 3	5.5	9 ± 2	19 ± 1	0.47
10× Phenol	68 ± 4	15 ± 2	4.5	11 ± 1	21 ± 1	0.52

[a] R is the ratio of $k_{target}/k_{nontarget}$.

compounds were listed in Table 2. As seen, the k_{app} values in real water sample were all lower than that in standard solutions: k_{app} value in tap water was slightly lower than that in standard solution, while k_{app} value in river water was substantially decreased. This phenomenon can be ascribed to the fact that the tested tap water was purified water, which was more similar to the standard solution in components. Some metal ions, organic compounds and salts existed in river water, which were easy to capture the photo-generated electrons, reduce photo-production holes or adsorb and scatter the radiation. As a result, the photolysis speed in river water was retarded. When 10 times of BPA or phenol was also spiked in those real water samples, k_{app} values displayed slight differences in standard solution and real water. This phenomenon may be explained as follows: the concentration of spiked BPA or phenol was far higher than the total amount of MIPs present in the real water, so the impact of material present in the real water on photocatalytic reaction could be ignored. Overall, the imprinted Fe_3O_4@SiO_2@TiO_2 (MIPs) displayed selective catalytic property in real water samples.

3.4. Reusability of the MIPs

The recovery and reusability of the photocatalyst are important in the photodegradation of organic pollutants, which is likely to be a key factor in improving the economic efficiency. To evaluate the lifetime of imprinted Fe_3O_4@SiO_2@TiO_2, the photodegradation of estrone (10 mg L^{-1}) was carried out in successive batches. During the experiments, the MIPs were simply recovered by external magnet. In the first cycle, the degradation was conducted by irradiating for 1 h. After separated and rinsed with distilled water to remove the residual estrone and byproducts, the MIPs were poured into the refreshed pollutant solution and then the irradiation was continued again for 1 h as the second cycle. This process was repeated and the kinetic data for parts of the degradation cycles are shown in Fig. 7. The results showed that the prepared MIPs could be used repeatedly at least 10 times without significant decrease in their k_{app} values. This indicated that the MIPs had excellent photochemical stability during the photodegradation process.

3.5. Comparison with other methods

Many excellent works about photodegradation of pollutants based on TiO_2 nanoparticles have been reported. Many strategies have been proposed to improve the photocatalytic activity of TiO_2 (ref. 25–29); for instance, MIPs based TiO_2 nanocomposites have been prepared in order to improve the selectivity of TiO_2 particles. Several typical examples about MIPs-TiO_2 were summarized in Table 3.[8–10,16,30–32] As can be seen from

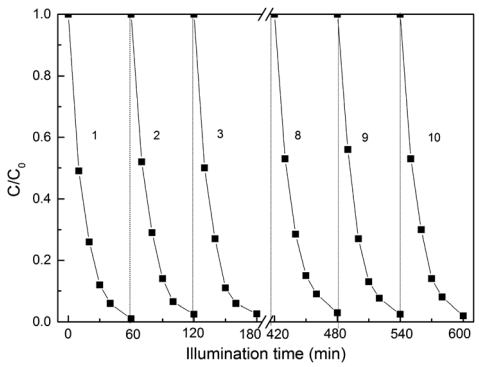

Fig. 7 Kinetic data for the repeated photocatalytic degradation of estrone over imprinted Fe_3O_4@SiO_2@TiO_2. The numbers were cycle number.

Table 2 Rate constants (k_{app}/min^{-1}) for the photocatalytic degradation of target pollutant (spiked estrone with 5.0 mg L^{-1}) in the presence of coexisted compounds over imprinted Fe_3O_4@SiO_2@TiO_2 in different real water samples

	Standard solution		Tap water		Ground water		River water	
	k_{target} ($\times 10^3$)	$k_{non\text{-}target}$ ($\times 10^3$)	k_{target} ($\times 10^3$)	$k_{non\text{-}target}$ ($\times 10^3$)	k_{target} ($\times 10^3$)	$k_{non\text{-}target}$ ($\times 10^3$)	k_{target} ($\times 10^3$)	$k_{non\text{-}target}$ ($\times 10^3$)
Estrone	85 ± 2	—	82 ± 2	—	79 ± 2	—	68 ± 3	—
10× BPA	61 ± 2	11 ± 3	61 ± 3	11 ± 4	60 ± 2	10 ± 2	57 ± 4	9 ± 3
10× phenol	68 ± 4	15 ± 2	68 ± 3	14 ± 3	67 ± 3	14 ± 2	63 ± 3	13 ± 2

Table 3 Comparison of MIP-coated photocatalysts for removal of organic pollutants

Photocatalysts	Target pollutant	Preparation method	Characteristic	Ref.
TiO_2@organic MIP	Chlorophenols Nitrophenols	In situ polymerization In situ polymerization	(1) Higher selectivity; (2) lower stability; (3) multistep procedure	8 9
TiO_2@inorganic MIP	Diethyl phthalate Dichlorophenol	Al^{3+} doping sol-gel method Cu^{2+} doping sol-gel method	(1) Higher stability; (2) mild polymerization conditions; (3) weak interaction between template and recognition sites	10 30
Matrices @imprinted TiO_2				
TiO_2/WO_3	4-Nitrophenol 2-Nitrophenol	One step sol-gel process	(1) Facile one-step sol-gel process	31
Glass	Salicylic acid	Liquid phase deposition	(1) Easy of template removal	16
TiO_2 NT	Anthracene-9-carboxylic acid	Surface sol-gel process	(1) Enhanced photocatalytic activity; (2) photostability	32
Fe_3O_4	Estrone	Liquid phase deposition	(1) Fast magnetic separation; (2) higher photocatalyst ability; (3) easy of template removal	This work

the table, selective removal of organic pollutants using directly imprinted TiO_2 matrices is a hopeful method. The Fe_3O_4@imprinted TiO_2 nanoparticles developed in this work exhibit high adsorption capacity, selectivity, and molecular recognitive photocatalytic activity for the target contaminant. Furthermore, it can provide fast separation ability, which is important for reuse of photocatalyst. So, the Fe_3O_4@imprinted TiO_2 nanoparticles are ideal candidates for photodegradation of pollutants.

4. Conclusions

In conclusion, estrone imprinted TiO_2 hybridized film was prepared by LPD method on the surface of magnetic Fe_3O_4 particles. The imprinted Fe_3O_4@SiO_2@TiO_2 could achieve selective adsorption and photodegradation of the target estrone over other organic pollutants. By simply changing template molecules, novel Fe_3O_4 surface imprinted TiO_2 can be prepared for other pollutants. Because of the high selectivity and excellent photocatalytic ability, the Fe_3O_4@imprinted TiO_2 has a promising prospect in the treatment of wastewater. In addition to the selectivity, another challenge problem for TiO_2 photocatalysis is the low utilization of visible light. The best source of light for photocatalyst is sunlight, which contains only a small part of ultraviolet light thereby improving the photocatalytic efficiency. Therefore, in future work, doping technique will be introduced to the process of depositing imprinted TiO_2 film. We anticipate to achieving selective photodegradation of the target pollutant by sunlight. Moreover, multiple contaminants always coexist in real water body, so photocatalytic process for multi-targets should be further investigated.

Acknowledgements

Financial support from the National Natural Science Foundation of China (21307052, 21275158), the Natural Science Foundation of Shandong Province of China (ZR2013BL006), and the Scholarship Award for Excellent Doctoral Student granted by the Ministry of Education of China, is gratefully acknowledged.

Notes and references

1 D. P. Grover, J. L. Zhou, P. E. Frickers and J. W. Readman, *J. Hazard. Mater.*, 2011, **185**, 1005–1011.
2 Z. Lin, Q. He, L. Wang, X. Wang, Q. Dong and C. Huang, *J. Hazard. Mater.*, 2013, **252–253**, 57–63.
3 M. C. Burleigh, M. A. Markowitz, M. S. Spector and B. P. Gaber, *Environ. Sci. Technol.*, 2002, **36**, 2515–2518.
4 S. Yi and W. Zhuang, *Environ. Sci. Technol.*, 2006, **40**, 2396–2401.
5 B. Sun, E. P. Reddy and P. G. Smirniotis, *Environ. Sci. Technol.*, 2005, **39**, 6251–6259.
6 D. Robert, A. Piscopo and J. V. Weber, *Sol. Energy*, 2004, **77**, 553–558.
7 O. V. Makarova, T. Rajh and M. C. Thurnaure, *Environ. Sci. Technol.*, 2000, **34**, 4797–4803.
8 X. Shen, L. Zhu, J. Li and H. Tang, *Chem. Commun.*, 2007, 1163–1165.
9 X. Shen, L. Zhu, G. Liu, H. Yu and H. Tang, *Environ. Sci. Technol.*, 2008, **42**, 1687–1692.
10 X. Shen, L. Zhu, C. Huang, H. Tang, Z. Yu and F. Deng, *J. Mater. Chem.*, 2009, **19**, 4843–4851.
11 S. F. Xu, H. Lu, X. Zheng and L. X. Chen, *J. Mater. Chem. C*, 2013, **1**, 4406–4422.
12 L. X. Chen, S. F. Xu and J. H. Li, *Chem. Soc. Rev.*, 2011, **40**, 2922–2942.
13 S. F. Xu, H. Lu, J. H. Li, X. Song, A. Wang, L. X. Chen and S. Han, *ACS Appl. Mater. Interfaces*, 2013, **5**, 8146–8154.
14 S. F. Xu, L. X. Chen, J. H. Li, Y. Guan and H. Lu, *J. Hazard. Mater.*, 2012, **237–238**, 347–354.

15 S. F. Xu, L. X. Chen, J. H. Li, W. Qin and J. Ma, *J. Mater. Chem.*, 2011, **21**, 12047–12053.
16 X. Shen, L. Zhu, H. Yu, H. Tang and S. Liu, *New J. Chem.*, 2009, **33**, 1673–1679.
17 J. Inoue, T. Ooy and T. Takeuchi, *Soft Matter*, 2011, **7**, 9681–9684.
18 Y. Li, Y. Li, L. Huang, Q. Bin, Z. Lin, H. Yang, Z. Cai and G. Chen, *J. Mater. Chem. B*, 2013, **1**, 1256–1262.
19 M. Tatemichi, M. Sakamoto, M. Mizuhata, S. Deki and T. Takeuchi, *J. Am. Chem. Soc.*, 2007, **129**, 10906–10910.
20 H. Deng, X. Li, Q. Peng, X. Wang, J. Chen and Y. Li, *Angew. Chem., Int. Ed.*, 2005, **44**, 2782–2785.
21 J. Ge, Q. Zhang, T. Zhang and Y. Yin, *Angew. Chem., Int. Ed.*, 2008, **47**, 8924–8928.
22 X. Wang, L. Wang, X. He, Y. Zhang and L. Chen, *Talanta*, 2009, **78**, 327–332.
23 C. D. Ki, C. Oh, S. Oh and J. Chang, *J. Am. Chem. Soc.*, 2002, **124**, 14838–14839.
24 X. Shen, L. Zhu, G. Liu, H. Tang, S. Liu and W. Li, *New J. Chem.*, 2009, **33**, 2278–2285.
25 G. Jiang, Z. Lin, L. Zhu, Y. Ding and H. Tang, *Carbon*, 2010, **48**, 3369–3375.
26 G. Jiang, Z. Lin, C. Chen, L. Zhu, Q. Chang, N. Wang, W. Wei and H. Tang, *Carbon*, 2011, **49**, 2693–2701.
27 Y. Chi, Q. Yuan, Y. Li, L. Zhao, N. Li, X. Li and W. Yan, *J. Hazard. Mater.*, 2013, **262**, 404–411.
28 C. Zhan, F. Chen, J. Yang, D. Dai, X. Cao and M. Zhong, *J. Hazard. Mater.*, 2014, **267**, 88–97.
29 L. Gu, J. Wang, Z. Zou and X. Han, *J. Hazard. Mater.*, 2014, **268**, 216–223.
30 D. M. Han, G. L. Dai, W. P. Jia and H. D. Liang, *Micro Nano Lett.*, 2010, **5**, 76–80.
31 X. Luo, F. Deng, L. Min, S. Luo, B. Guo, G. Zeng and C. Au, *Environ. Sci. Technol.*, 2013, **47**, 7404–7412.
32 Y. Liu, R. Liu, C. Liu, S. Luo, L. Yang, F. Sui, Y. Teng, R. Yang and Q. Cai, *J. Hazard. Mater.*, 2010, **182**, 912–918.

